Ultrahigh-resolution, high-speed spectral domain optical coherence phase microscopy

Rehman Ansari,[1,*] Christian Myrtus,[1] Redouane Aherrahrou,[3] Jeanette Erdmann,[3] Achim Schweikard,[2] and Gereon Hüttmann[1,4]

[1]*Institute for Biomedical Optics, University of Lübeck, Germany*

[2]*Institute for Robotics and Cognitive Systems, University of Lübeck, Germany*

[3]*Institute for Integrative and Experimental Genomics, University of Lübeck, Germany*

[4]*Member of the German Center for Lung Research (DZL), Germany*

**Corresponding author: ansari@rob.uni-luebeck.de*

Received September 23, 2013; revised November 15, 2013; accepted November 18, 2013; posted November 19, 2013 (Doc. ID 196949); published December 19, 2013

We present an ultrahigh-resolution, high-speed spectral domain optical coherence phase microscopy (SD-OCPM) system that combines submicrometer transverse spatial resolution and subnanometer optical path length sensitivity, with an acquisition speed of over 217,000 voxels/s. The proposed SD-OCPM system overcomes two significant drawbacks of traditional common-path interferometers—limited transverse spatial resolution and suboptimal detection sensitivity—while maintaining phase stability that is comparable with common-path interferometer setups. The transverse and axial spatial resolution of the setup is measured to be 0.6 and 1.9 μm, respectively, with a phase sensitivity of 0.0027 rad (corresponds to optical path length sensitivity of 110 pm). High-speed acquisition allows for phase-sensitive 4D imaging of biological samples with subcellular resolution.

OCIS codes: (180.6900) Three-dimensional microscopy; (110.0180) Microscopy; (110.1650) Coherence imaging; (170.0180) Microscopy; (170.6900) Three-dimensional microscopy.

http://dx.doi.org/10.1364/OL.39.000045

Optical coherence phase microscopy (OCPM) [1,2] is a powerful imaging technique that quantitatively measures subnanometer displacements of depth scatterers in a sample. OCPM has been demonstrated to be useful in label-free detection of biomolecular interactions [3], detection of action potentials in nerve bundles [4], the measurement of contraction dynamics in beating cardiomyocytes [5], etc. Generally, OCPM has been implemented using common-path interferometers, as it provides very high phase sensitivity [2,3,6–11]. However, common-path topologies have two significant drawbacks: limited transverse spatial resolution and suboptimal detection sensitivity. In common-path interferometer setups, specular reflection from a surface near the sample provides the reference electromagnetic field, which interferes with backscattered light from the sample to produce an interference fringe pattern. A smaller numerical aperture (NA) scanning optics or larger depth of field are required to get reflections from both the reference surface (generally a glass coverslip) and the sample, which in turn limits the transverse spatial resolution. The suboptimal detection sensitivity results from the fixed reference light intensity, which cannot be easily adjusted to obtain an optimum signal-to-noise ratio (SNR), which is an important imaging parameter. Recently, these issues were addressed with a dual sample arm beam setup, where two beams with large and small diameters and different polarization states were formulated in the sample arm and focused on the sample and glass coverslip, respectively [12]. However, the proposed setup was relatively complex, required a glass coverslip positioned close to the sample, and the achieved phase sensitivity was only 0.021 rad.

Here we describe a high-speed spectral domain OCPM (SD-OCPM) system that overcomes the limitations of common-path interferometer setups and combines high NA imaging with OCPM. Our setup did not require a glass coverslip positioned close to the sample, and a high working distance (3.1 mm) allowed for OCPM imaging of both cell cultures and biological tissues. The implemented SD-OCPM system provided submicrometer transverse spatial resolution and subnanometer axial path length sensitivity with an acquisition speed of over 217,000 voxels/s. The SD-OCPM system was implemented with a symmetric Linnik interferometer formed by a pair of identical 0.8 NA microscope objectives and a nonpolarizing beam splitter. A pair of XY-galvanometer scanners was used to scan laterally through the beam splitter. The scanning beam split into a reference and sample arm after the galvanometer scanners, which made the interference fringe recording insusceptible to the jitter and vibrational noise of the galvanometer scanners, which are major sources of vibrational noise in OCPM setups. The Linnik interferometer was mechanically isolated from the rest of the setup and stationed on a passively damped optical table to improve further the phase sensitivity.

The SD-OCPM system was integrated into a widefield microscope for better visualization of the sample under focus, as shown in Fig. 1. A high-power superluminescent diode (SLD; Superlum Inc., Ireland) was used as the light source for the SD-OCPM, with an 835 nm center wavelength, 54 nm FWHM bandwidth, and 29 mW output power. The light from the SLD was coupled into the optical setup with a 50/50 fiber coupler. After the galvanometer scanners, the light passed through a 1:2 telescopic relay, which increased the beam diameter to 8 mm, so as to completely fill the back aperture of 0.8 NA water-immersion microscope objectives (Achroplan 40× IR, Carl Zeiss Microimaging GmbH). The telescopic relay also imaged the midplane between the XY-scanners' pivot points onto the exit pupil planes of the microscope objectives. A gold-plated mirror with $\lambda/10$ surface quality was used in the reference arm,

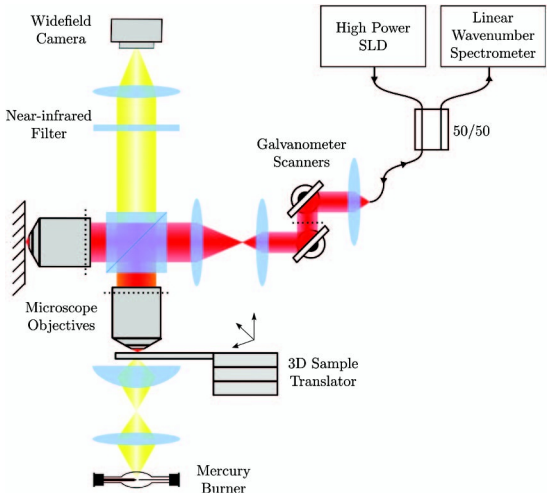

Fig. 1. Schematic overview of the integrated widefield microscope and spectral domain OCPM system.

and a special mirror holder was designed to keep the gold mirror and microscope objective of the reference arm immersed in water. A linear wavenumber spectrometer was used to record the spectrally resolved interferograms, using a high-speed line scan camera (spL4096-140 k, Basler AG) with a readout speed of 217,000 lines/s. Since the recorded interferograms were uniformly spaced in k space, computationally intensive data interpolation was not required before taking the Fourier transform, which increased the overall volumetric image reconstruction speed. A 3D sample translation stage was used for positioning the sample under the microscope. The translation stage was constructed using a pair of piezo motors (M-663, Physik Instrumente GmbH) for lateral translation and a linear motor (M-125, Physik Instrumente GmbH) for axial translation. Custom software was developed in LabVIEW (National Instruments) to read out the spectral interferograms and synchronize them with the galvanometer scanners and 3D sample translation stage.

Because of the high NA of the objective lens, the depth of field (1.1 μm) was much smaller than the coherence length (5.8 μm) of the light source. Therefore, the axial response of the system was determined by the convolution between the coherence gated response of the broadband light source and the confocal gated response of the objective lens. The combination of the confocal and coherence gating rejected out-of-focus and multiple-scattered light much more effectively than the confocal gating alone and enabled optical sectioning in highly scattering media, such as biological tissues. The axial and transverse spatial resolution determined by measuring the three-dimensional point spread function was 2 and 0.6 μm, respectively, which was in close agreement with the theoretical values of 1.9 and 0.4 μm, respectively. The submicrometer transverse spatial resolution of the system is demonstrated by scanning the groups 8 and 9 line pairs of the Air Force resolution target (Fig. 2). The finest line pairs of group 9 are separated by 0.78 μm. Figure 2 also shows the depth profile of the line pairs, which was obtained by unwrapping the two-dimensional phase image. The SD-OCPM system can cover a maximum field of view of 0.72 mm in diameter with submicrometer spatial resolution. The temporal

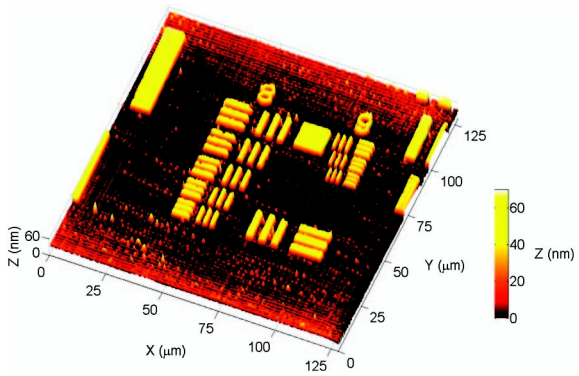

Fig. 2. Three-dimensional profile of an Air Force resolution target with groups 8 and 9 line pairs clearly visible. Color bar represents the height of the metal deposit in nanometers.

resolution of the system can be adjusted in relation with the image field size, with up to 108 subvolumes/s for a 30 μm × 30 μm image field size with 1 μm/pixel.

The interferometric phase of coherently detected backscattered light can be represented as

$$\phi = 2k_0(n\Delta l), \tag{1}$$

where k_0 is the center wavenumber of the light source, n is the sample refractive index, and Δl is the optical path length difference between the sample and reference arms, which corresponds to a fixed depth position inside the sample as the reference path length is fixed. The interferometric phase is sensitive to the motions of the depth scatterers in a sample or the variations in an optical index. The minimum change in the optical path length of the depth scatterers that can be measured is limited by the stability of the interferometric phase measurements, which is calculated by taking the standard deviation of the phase difference values over time. For a shot-noise limited-detection system, the theoretical limit of phase stability is determined by the SNR given as [13,14]

$$\delta\phi_{\text{sens}} \propto \frac{1}{\sqrt{\text{SNR}}}. \tag{2}$$

The phase sensitivity of the SD-OCPM setup was measured as 0.0027 rad (0.1 nm optical path length sensitivity) at 56 dB of SNR, whereas the theoretical limit on the phase sensitivity at 56 dB of SNR determined from Eq. (2) was 0.0016 rad. The dominating noise source was determined to be the galvos by comparing the theoretical and measured phase sensitivities of the setup without the galvos.

The implemented SD-OCPM system combines submicrometer transverse spatial resolution with subnanometer optical path length sensitivity, which can be utilized for the quantitative measurement of cellular dynamics. This capability is demonstrated by measuring the axial displacement of subcellular structures in spontaneously beating cardiomyocyte cells. Mouse embryonic stem cells were differentiated into cardiomyocyte cells through the formation of embryoid bodies [15]. Complex *en face* images were obtained by taking the Fourier transform of offset-corrected and apodized interferograms

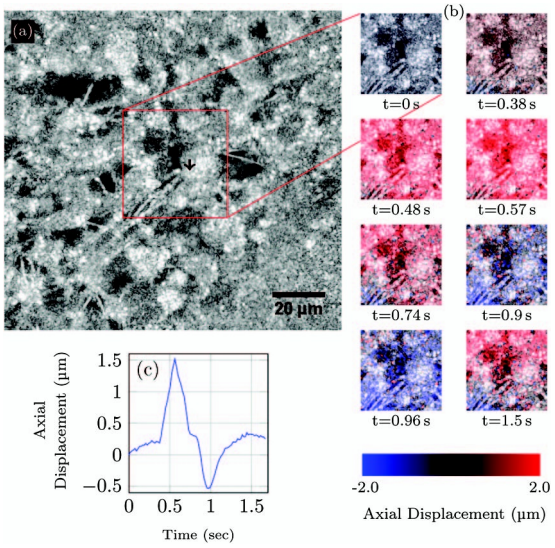

Fig. 3. Images of spontaneously beating cardiomyocyte cells. (a) *En face* image; (b) time lapse images of a 40 μm × 40 μm area, color coded with axial displacement resulting from spontaneous contraction (Media 1). (c) Axial displacement profile of cell membrane on location marked by an arrow in image (a).

and slicing the A-scans along the focal plane. Amplitude and phase images were obtained by computing the absolute and phase angle values of complex *en face* images, respectively. The phase images were unwrapped over time and scaled into axial displacement given as

$$z = \frac{\phi}{4n\pi}\lambda_o, \tag{3}$$

where ϕ is the unwrapped phase, λ_o is the center wavelength of the light source, and n is the refractive index of the sample.

Figure 3(a) shows an *en face* amplitude image of cardiomyocyte cells, (b) (Media 1) shows a 40 μm × 40 μm area scanned at 54 frames/s, color coded with axial displacement values at different instances of time during the spontaneous beating cycle, and (c) shows the axial displacement profile of the cell membrane. The spatiotemporal changes in the axial displacement values help visualize the initiation and progression of the contraction wave as it propagates through the cardiomyocyte cells.

In summary, an ultrahigh-resolution high-speed spectral domain OCPM system is presented, which overcomes the limited transverse spatial resolution drawback of common-path interferometer setups and enables phase-sensitive imaging of subcellular structures. The implemented SD-OCPM system combines submicrometer transverse spatial resolution with subnanometer optical path length sensitivity, with an acquisition speed of over 217,000 voxels/s. A three-dimensional structure of biological samples with subcellular resolution can be reconstructed by acquiring a stack of *en face* images at different depths. In addition, subnanometer optical path length sensitivity enables the spatiotemporal measurement of cellular dynamics, such as the detection of action potentials in neurons, an application that we are currently investigating.

This work was supported by the Graduate School for Computing in Medicine and Life Sciences funded by Germany's Excellence Initiative (DFG GSC 235/1), the Airway Research Center North (ARCN), which is part of the German Center for Lung Research (DZL).

References

1. C. G. Rylander, D. P. Davé, T. Akkin, T. E. Milner, K. R. Diller, and A. J. Welch, Opt. Lett. **29**, 1509 (2004).
2. M. A. Choma, A. K. Ellerbee, C. Yang, T. L. Creazzo, and J. A. Izatt, Opt. Lett. **30**, 1162 (2005).
3. C. Joo, E. Özkumurc, M. S. Ünlüc, and J. F. de Boer, Biosens. Bioelectron. **25**, 275 (2009).
4. T. Akkin, D. P. Dav, T. E. Milner, and H. G. Rylander III, Opt. Express **12**, 2377 (2004).
5. A. K. Ellerbee, T. L. Creazzo, and J. A. Izatt, Opt. Express **15**, 8115 (2007).
6. C. Joo, T. Akkin, B. Cense, B. H. Park, and J. F. de Boer, Opt. Lett. **30**, 2131 (2005).
7. M. A. Choma, A. K. Ellerbee, S. Yazdanfar, and J. A. Izatt, J. Biomed. Opt. **11**, 024014 (2006).
8. S. M. Motaghian Nezam, C. Joo, G. J. Tearney, and J. F. de Boer, Opt. Express **16**, 17186 (2008).
9. A. St. Quintin, L.-K. Merhi, and M. V. Sarunic, Appl. Opt. **50**, 1798 (2011).
10. I. Shock, A. Barbul, P. Girshovitz, U. Nevo, R. Korenstein, and N. T. Shakeda, J. Biomed. Opt. **17**, 101509 (2012).
11. P. O. Bagnaninchi, C. Holmes, and M. Tabrizian, Proc. SPIE **8580**, 85800E (2013).
12. F. Helderman, B. Haslam, J. F. de Boer, and M. de Groot, Opt. Lett. **38**, 431 (2013).
13. S. Yazdanfar, C. Yang, M. V. Sarunic, and J. A. Izatt, Opt. Express **13**, 410 (2005).
14. B. H. Park, M. C. Pierce, B. Cense, S. H. Yun, M. Mujat, G. J. Tearney, B. E. Bouma, and J. F. de Boer, Opt. Express **13**, 3931 (2005).
15. V. A. Maltsev, A. M. Wobus, J. Rohwedel, M. Bader, and J. Hescheler, Circ. Res. **75**, 233 (1994).